Neuronal Hyperactivity Accelerates Depletion of Neural Stem Cells and Impairs Hippocampal Neurogenesis

Amanda Sierra[1,2,3], **Soraya Martín-Suárez**[1], **Roberto Valcárcel-Martín**[1], **Jesús Pascual-Brazo**[5], **Sarah-Ann Aelvoet**[4], **Oihane Abiega**[1], **Juan J. Deudero**[5], **Amy L. Brewster**[5], **Irantzu Bernales**[3], **Anne E. Anderson**[5], **Veerle Baekelandt**[4], **Mirjana Maleti -Savati** [5,*], and **Juan M. Encinas**[1,2,3,*]

[1]Achucarro Basque Center for Neuroscience, Laida Bidea 205, 48170 Zamudio, Spain

[2]Ikerbasque Foundation, María Díaz de Haro 3, 6th Floor, 48013 Bilbao, Spain

[3]University of the Basque Country (UPV/EHU), Barrio Sarrena s/n, 48940 Leioa, Spain

[4]KU Leuven, Oude Markt 13, 3000 Leuven, Belgium

[5]Baylor College of Medicine, The Jan and Dan Duncan Neurological Research Institute at Texas Children's Hospital, 1250 Morsund St., Houston, TX 77030, USA

SUMMARY

Adult hippocampal neurogenesis is believed to maintain a range of cognitive functions, many of which decline with age. We recently reported that radial neural stem cells (rNSCs) in the hippocampus undergo activation-dependent conversion into astrocytes, a mechanism that over time contributes to a reduction in the rNSC population. Here, we injected low and high levels of kainic acid (KA) in the dentate gyrus to assess whether neuronal hyperexcitation, a hallmark of epileptic disorders, could accelerate this conversion. At low levels of KA, generating epileptiform activity without seizures, we indeed found increased rNSC activation and conversion into astrocytes. At high levels, generating sustained epileptic seizures, however, we find that rNSCs divide symmetrically and that both mother and daughter cells convert into reactive astrocytes. Our results demonstrate that a threshold response for neuronal hyperexcitation provokes a dramatic shift in rNSCs function, which impairs adult hippocampal neurogenesis in the long term.

Graphical Abstract

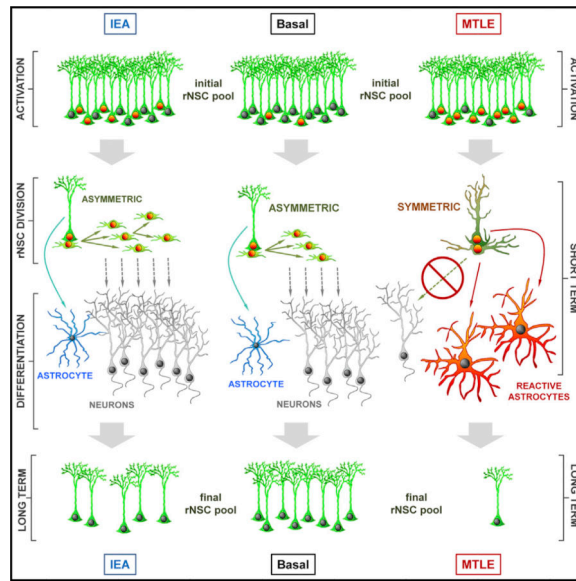*Correspondence: maletics@bcm.edu (M.M.-S.), jm.encinas@ikerbasque.org (J.M.E.).

INTRODUCTION

Adult neurogenesis (Altman and Das, 1965) persists in the adult hippocampus of most mammals, including humans (Eriksson et al., 1998; Spalding et al., 2013). In the subgranular zone (SGZ) of the dentate gyrus (DG), newly born neurons migrate to become integrated in the mature granule cell synaptic circuitry (van Praag et al., 2002), which from the hippocampus projects to itself and other areas of the brain. Their ability to modulate the existing network to influence pattern separation is believed to encode context that underlies formation of distinct memories (Sahay et al., 2011). Because of its important role in memory formation and learning, impairment of adult hippocampal neurogenesis leads to deficits in hippocampus-dependent learning tasks (Clelland et al., 2009; Deng et al., 2009; Dupret et al., 2008; Farioli-Vecchioli et al., 2008; Imayoshi et al., 2008; Saxe et al., 2006). In addition, mood disorders such as anxiety and depression are affected by hippocampal neuroendocrine regulation and become exacerbated when adult neurogenesis is inhibited (Snyder et al., 2011).

New neurons arise from a population of glia-like radial neural stem cells (rNSCs), that, like astrocytes, express glial fibrillary acid protein (GFAP) (Fukuda et al., 2003; Seri et al., 2001). rNSCs divide mostly asymmetrically, giving rise to rapidly proliferating amplifying neural progenitors (ANPs) that lack GFAP expression and differentiate into neurons (Kempermann et al., 2004). Overproduction of ANPs is kept in check by apoptosis and microglial phagocytosis (Sierra et al., 2010). Most neurogenic stimuli reported to date, from physical activity to antidepressants (Kronenberg et al., 2003; Encinas et al., 2006, 2011a; Hodge et al., 2008), are known to target the ANP population, whereas mechanisms that specifically control quiescence and activation of rNSCs have been more challenging to identify.

Early work had suggested that strong enhancers of neuronal activity such as electroconvulsive shock (Segi-Nishida et al., 2008) and systemic injection of kainic acid

(KA), a glutamate agonist, increase activation of rNSCs (Hüttmann et al., 2003). More recently, epileptic seizures were found to activate and expand a subset of quiescent rNSCs that were distinct from those activated by running (Lugert et al., 2010). Using optogenetic approaches, Song et al. (2012) found that rNSCs depend on tonic release of GABA from fast-spiking parvalbumin interneurons to make dynamic choices between activation and self-renewal modes, as well as return to quiescence. The transcription factor Ascl1 has been proposed to be a main molecular link between neuronal activity and rNSC activation (Andersen et al., 2014). These recent findings suggest that activation of quiescent rNSCs is controlled directly by the level of activity of the surrounding hippocampal neural network, with important implications for pathological conditions of neuronal hyperactivation such as epilepsy. Indeed, it is known that epileptic seizures can chronically impair hippocampal neurogenesis (Hattiangady et al., 2004; Mathern et al., 2002; Paradisi et al., 2010; Pirttilä et al., 2005). In turn, impaired neurogenesis has been suggested to contribute to the cognitive deficits (Gargaro et al., 2013) and the psychiatric comorbidities (Heuser et al., 2009) associated with mesial temporal lobe epilepsy (MTLE), a chronic condition in which a third of patients do not respond to medical treatment. Neuronal alterations, as well as reactive astrocytosis, have been proposed as an underlying mechanism driving both pathology and endogenous repair in epileptogenesis (Gibbons et al., 2013), the extent to which rNSCs as well may participate in these processes is not known.

We reported earlier that under normal conditions and at the population level rNSCs have restricted mitotic potential; once they are activated to enter the cell cycle they undergo a round of several consecutive asymmetric cell divisions to generate neuronal precursors and immediately thereafter differentiate into astrocytes (Encinas et al., 2011b). Thus, rNSCs deplete over time after being activated, a mechanism accounting for most of the age-associated decline of hippocampal neurogenesis. Indeed, blocking rNSC activation through Acl1 knockout prevents the age-associated decline of the rNSC pool (Andersen et al., 2014).

In the present study, we asked whether neuronal hyperexcitation in the hippocampus would intensify rNSC activation and accelerate their normal aging-related depletion, prematurely exhausting hippocampal neurogenesis. We also asked whether distinct levels of neuronal hyperexcitation would elicit disparate responses on rNSCs and the neurogenic niche. Using constitutive and conditional nestin-based reporter transgenic mice, we performed intrahippocampal injections of high and low doses of KA to model MTLE (Bouilleret et al., 1999), as well as epileptiform activity (EA), neuronal hyperexcitation discharges in the form of waves and spikes that do not trigger seizures, but are detectable by electroencephalographic (EEG) recordings in epilepsy patients. We find in both models that rNSC activation is increased and rNSC depletion accelerated, but both elicit distinctly different self-renewal modes.

RESULTS

Intrahippocampal Injection of KA Mimics MTLE and EA

In order to test distinct levels of neuronal hyperactivity in a precisely controlled manner, we resorted to KA, which can be delivered locally into the DG accurately titrated (Figure 1) to consistently reproduce the human pathophysiological features of MTLE: unprovoked

seizures and hippocampal sclerosis, including cell death, gliosis, inflammation, and granule cell dispersion (GCD) (Babb et al., 1995; Bouilleret et al., 1999; Heinrich et al., 2006; Kralic et al., 2005; Nitta et al., 2008). We confirmed the seizure-inducing effect of 1 nmol of KA in 50 nl of saline (MTLE mice) injected into the DG of Nestin-GFP transgenic mice (Mignone et al., 2004), in which rNSCs and ANPs are readily visualized in the SGZ (Figure 1A). EEG recordings from the hippocampus confirmed that MTLE mice developed seizures (repetitive-spike and slow-wave discharges lasting 10 s or more) within 6 hr after the KA injection and later generated seizures spontaneously for the duration of the recording, which lasted up to 50 days (Figures 1B–1D). In addition to seizures, MTLE mice also had interictal discharges, determined as fast and high amplitude spike events lasting up to 200 ms (Figures 1B–1E). The electrographic seizures in MTLE mice were synchronized with behavioral stage 4–5 generalized seizures (monitored by video recording) according to the Racine scale (Racine, 1972), with forelimb clonus, rearing, and falling (data not shown). In addition to the MTLE, we developed a model to mimic the EA that occurs between seizures. For this purpose, we injected a lower dose of KA (0.037 nmol in 50 nl of saline) into the DG of Nestin-GFP mice (EA mice). EA mice did not develop seizures at any time point, but as early as 6 hr after the KA injection they showed epileptiform discharges that continued intermittently for the duration of the recordings (Figure 1B). The frequency of interictal epileptiform discharges was significantly higher in the MTLE group as compared with the EA group (Figure 1E). Saline-injected controls (Sal mice) did not display seizures or EA at any time during the monitoring. In addition to seizures and interictal spikes, MTLE is also characterized by a number of pathological changes in the DG. Accordingly, we found significantly increased GCD and decreased GC density in MTLE mice (Figures 1F–1I) compared with Sal and EA mice, while no difference was found between the latter two groups.

We also measured inflammation at 1- and 3-day post-KA injection (dpKAi) by determining the expression of mRNA from several cytokines (Figure 1J). At 1 dpKAi, MTLE mice significantly overexpressed interleukin-1β (IL-1β), interleukin 6 (IL-6), tumor necrosis factor α (TNF-α), and transforming growth factor β (TGF-β) compared with Sal mice. IL-6, TNF-α, and TGF-β mRNA levels were also significantly higher in the MTLE group in comparison to the EA group. At this time point, IL-6 and TNF-α were significantly higher in EA mice compared with Sal mice. At 3 dpKAi, however, all the analyzed cytokines were significantly overexpressed in MTLE mice when compared with Sal and EA mice, but no difference was found between the latter two groups (Figure 1J).

To further explore our EA model, we performed genome-wide expression analysis of the DG from Sal, EA, and MTLE mice at 3 dpKAi by means of a two-color gene microarray (Figure S1). We found that the expression changes induced by EA were subtle and not significant compared with the Sal group when using conventional statistical criteria (for a sample size = 4), and thus, more permissive statistical criteria were used (Figure S1A). To investigate the functional relevance of the changes induced by EA and MTLE, we performed pathway and gene ontology enrichment analyses. We found that MTLE induced a robust overexpression of pathways involved in matrix remodeling; cellular damage (unfolded protein response, stress, and apoptosis); activation of the cellular and humoral branches of the immune system; activation of the cell cycle; metabolism; and signaling

pathways such as Notch, semaphorin 4b, and the erbB tyrosine kinase receptor (Figure S1B; Table S1). MTLE also induced a robust downregulation of pathways related to neurotransmitter receptor and signaling (mostly related to ionotropic glutamate receptors); glycosphingolipid and nitric oxide metabolism; as well as signaling pathways related to nodal/activin, hedgehog, and other components of the erbB pathway (Figure S1C; Table S2). Most of the changes induced by EA were also induced by MTLE (genes with common regulation), including upregulation of pathways related to the cell cycle or the immune response (Figure S1C; Table S3), and downregulation of a few genes, for which functional analysis could not be performed (Table S4). In addition, EA specifically induced changes in the expression of few genes that were not modified by MTLE and were not functionally related (Tables S5 and S6).

These results show that our EA model triggers a subtle response in the DG and therefore is a unique tool to study changes in rNSCs directly related to neuronal hyperactivity, whereas, as expected, MTLE provokes a strong pathological response.

Both EA and MTLE Increase Cell Proliferation in the Short Term and Activate rNSCs

Our hypothesis predicts that different levels of neuronal hyperactivity will lead to different amounts of rNSC and ANP activation. To test this prediction, we first determined the number of cells which were in cell cycle, measured as Ki67-positive cells in the SGZ and the GCL together. Proliferation was significantly increased in EA mice (both at 3 and 7 dpKAi) and MTLE mice (at 3 dpKAi), but was later (at 50 and 150 dpKAi) decreased below the Sal group levels (Figures S2A–S2C). We then used the thymidine analog 5-bromo-2′-deoxyuridine (BrdU), a tool that allows the analysis of cell proliferation as well as of survival and differentiation. In agreement with previous reports, a very low proportion of rNSCs were in S phase ($3.29\% \pm 0.44\%$) in the Sal group after a short pulse (BrdU was given at 2 dpKAi and the mice were sacrificed 2 hr later). In contrast, there were significant increases in the EA ($7.62\% \pm 0.18\%$) and MTLE (14.87 ± 1.32) groups (Figure S2D). The same changes in cell proliferation in EA and MTLE mice compared with the Sal group were observed when measured with Ki67 (Figure S2E).

To determine which cell types were proliferating in the DG, we administered BrdU to Nestin-GFP mice at 2 or 6 dpKAi and sacrificed the animals 24 hr later. The number of activated (BrdU-positive) rNSCs was notably higher in MTLE mice at 3 and 7 dpKAi (Figures 2A–2D). Interestingly, MTLE did not induce ANP proliferation at 3 or 7 dpKAi. In fact, the number of proliferating ANPs was reduced in MTLE mice compared to both Sal and EA mice (Figures 2A and 2B). In contrast, EA increased not only the activation of rNSCs at 3 and 7 dpKAi (although more modestly than MTLE), but also the proliferative activity of ANPs at both time points (Figures 2A and 2B).

Importantly, dividing astrocytes (BrdU$^+$GFAP$^+$ Nestin-GFP$^-$ cells) were rarely observed, and their number was not altered in EA or MTLE mice (Figures 2A–2D). BrdU$^+$ cells were almost completely restricted to the SGZ in Sal and EA mice, but in MTLE mice, dividing cells were also found in the hilus and the molecular layer (these cells were excluded from the quantification, Figure 2E). In conclusion, MTLE induced a rapid and massive activation

of rNSCs to enter the cell cycle whereas EA induced a more modest but still significant activation of rNSCs and also promoted ANP proliferation.

rNSCs Become Reactive and Divide Symmetrically in MTLE

Remarkably, in MTLE, rNSCs not only became activated in large numbers, but they also changed both their morphology and their cell-cycle program. At 3 dpKAi, we observed that the majority of the rNSCs presented a "reactive phenotype" (Figures 2 and 3), following similar criteria used to describe reactive astrocytes (Sofroniew and Vinters, 2010): In contrast to the typical single radial process that characterizes rNSCs in normal conditions (Figure 3A), several primary processes emerged from an enlarged soma of the rNSCs of MTLE mice. In addition, the processes were also significantly thicker, and there was a clear increased expression of both Nestin-GFP and GFAP. Finally, secondary branching, especially in the initial segment of the primary process, was noticeable in the rNSCs of MTLE mice (Figures 3A–3C). The quantification of these morphological parameters (number and thickness of the primary processes, and secondary branching) showed significant differences (Figures 3D–3F). No differences in rNSC morphology were identified in EA and Sal mice. Thus, after seizures, rNSCs acquire a reactive phenotype that shares features with that of reactive astrocytes: increased ramification, hypertrophic cell body, thickened prolongations, and overexpression of nestin and GFAP.

We also observed that in MTLE mice most of the daughter cells of reactive rNSCs presented a similar phenotype to that of the mother cell, suggesting that seizures prompt a switch from predominantly asymmetric rNSC division in normal conditions to symmetric division (Figures 3G–3L). We modified slightly our experimental paradigm for BrdU administration to investigate this functional switch in the type of cell division of rNSCs in detail. Nestin-GFP mice were intrahippocampally injected with Sal or KA and at 2 dpKAi were administered BrdU (four injections 2 hr apart). The animals were sacrificed 16 hr after the first BrdU injection (Figure 3G), a period shorter than the estimated time needed to complete mitosis (Hayes and Nowakowski, 2002; Encinas et al., 2011b) so that we could unambiguously identify rNSCs undergoing division (in the stages of telophase, karyokinesis, or cytokinesis) and characterize the morphological and marker-expression features of the daughter cell. Thus, we analyzed only BrdU-stained pairs of cells in which the nuclei of the rNSC and its daughter cell were in contact and their cytoplasms were still united. Under normal conditions and as we confirmed in the Sal and EA mice, rNSCs divide mostly asymmetrically, giving rise to ANPs that bear only very short (1–5 μm) and thin (1–2 μm) processes and lack GFAP expression (Figures 3I and 3J). In contrast, in MTLE mice, we observed that daughter cells being born from reactive rNSCs had long (10–50 μm) and thick (3–5 μm) processes strongly immunostained for GFAP (Figures 3K and 3L). Thus, in contrast to the asymmetric neurogenic model of division that takes place in normal conditions and in Sal and EA mice, we here demonstrate a symmetrical model of division of rNSCs in which both the mother and daughter cell differentiate into reactive astrocytes at the time of cell division. Thus, rNSCs in the MTLE mice shift to a mode of symmetrical division in which both the mother and daughter cell differentiate into reactive astrocyte-like cells.

These experiments strongly suggest that seizures trigger an early switch in rNSCs to directly differentiate into reactive astrocytes in parallel with cell division. To further test this hypothesis, we used inducible genetic fate-mapping employing tamoxifen-inducible Nestin-Cre-ER^{T2}/R26R:YFP transgenic mice (Lagace et al., 2007). First, we analyzed in which cell types the expression of YFP was activated 3 days after tamoxifen induction. As expected, the vast majority of the YFP-expressing cells were rNSCs, and low numbers of ANPs and neuroblasts were detected (Figures 4A and 4B).

We next performed a tight-criteria short-term lineage analysis of YFP-expressing cells in the Nestin-Cre-ER^{T2}/R26R:YFP Sal and MTLE mice at 1 and 3 dpKAi. We focused on pairs of YFP-expressing cells, joined by the cytoplasm, whose nuclei could be unambiguously identified less than 5 μm apart so that there was no doubt that the pairs of cells originated through cell division (Figures 4C–4E). One of the cells had to be GFAP positive and with rNSC morphology. The analysis was performed at 1 and 3 dpKAi. In Sal mice, the majority of the rNSC-containing clones were derived from an asymmetric division generating an rNSC and an ANP. In MTLE mice at 1 dpKAi, however, a significantly increased proportion of rNSC-derived clones was formed by an rNSC and a GFAP-expressing cell with long processes (Figure 4F). Remarkably, at 3 dpKAi, most of the clones belonged to this symmetric-division category (Figure 4G).

Inflammatory Response Alone Does Not Activate rNSCs

We next considered the possibility that rNSCs may become reactive not because of neuronal hyperactivity in MTLE mice, but because of the inflammation provoked by seizures. To test this possibility, we injected lipopolysaccharide (LPS) directly into the hippocampus of Nestin-GFP mice and compared rNSC morphology and activation with that observed in the Sal, EA, and MTLE mice. LPS triggered an overall increase in cell proliferation, as measured by incorporation of BrdU. In the SGZ + GCL of LPS mice, however, the absolute number of proliferating cells was significantly lower than in the other groups (Figures S3A–S3C). The proportion of activated rNSCs was also significantly lower, especially when compared with the MTLE group (Figures S3D–S3F). In addition, no morphological changes were observed in the rNSCs in LPS-injected mice. These results strongly indicate that inflammation alone is not sufficient to elicit the rNSC response to seizures observed in MTLE mice.

EA and MTLE Both Deplete rNSCs

According to our hypothesis, increased activation of rNSCs would noticeably accelerate the depletion of the rNSC population over time. We therefore quantified the total number of rNSCs at 3, 50, and 150 dpKAi (Figure 5). No significant changes were observed at 3 dpKAi; in contrast, at 50 and 150 dpKAi, a significantly reduced number of rNSCs was found in both EA and MTLE mice compared with the Sal group. Strikingly, the population of rNSCs was almost completely depleted at 150 dpKAi in the MTLE mice (Figure 5A), and the DG showed marked gliosis, with a massive presence of reactive astrocytes (Nestin-GFP-positive hypertrophic astrocytes with thickened processes overexpressing GFAP) (Figures 5A–5D). EA mice also had a significantly reduced population of rNSCs at 150 dpKAi, but the DG was otherwise normal (Figures 5B and 5C). These results demonstrate that the

intensified rNSC activation provoked by EA and, more robustly, by MTLE correlates with an accelerated depletion of the rNSC population.

To rule out the possibility that this depletion was caused by cell death, we measured the number of apoptotic cells (cells expressing activated-caspase 3 with pyknotic/karryorrhectic nuclei). The number of apoptotic cells in the DG at 1 and 3 dpKAi was significantly higher in MTLE mice than in Sal and EA mice (Figures S4A–S4D). Further detailed analysis demonstrated that in MTLE, but not in EA mice, there was an increase in apoptotic rNSCs, ANPs, and astrocytes (Figures S4E–S4I). However, the number of apoptotic rNSCs was very low and represented only a very small fraction of the total number of apoptotic cells, largely comprised of neuroblasts and GCs (Figures S4H–S4J). Thus, the rNSC population was therefore not exhausted by apoptosis.

EA and MTLE Both Impair Neurogenesis in the Long Term

We next sought to investigate whether the depletion of rNSCs translated into impaired neurogenesis. We resorted to a classical BrdU pulse-and-chase paradigm (Figures 6 and S5). BrdU was given at 2 dpKAi (when the maximum increase in rNSC division occurs), and the animals were sacrificed at 50 dpKAi. The absolute number of newborn BrdU-positive cells was significantly higher in both the EA and MTLE mice than in the Sal group. Interestingly, the total number of newly generated neurons (BrdU$^+$NeuN$^+$ cells) was increased in EA mice, while it was drastically diminished in MTLE mice (Figure 6A). Most of the newborn neurons found in MTLE mice were located in the hilus (Figure 6C), which indicates aberrant neurogenesis (Parent et al., 2006). Because the number of newborn astrocytes was also increased in EA mice (measured as BrdU$^+$GFAP$^+$ cells; Figures 6A and 6D; and as BrdU$^+$S100-β^+ cells; data not shown), the relative proportion of new neurons and astrocytes in these mice these mice was not was not different from the Sal group (Figure S5A). These results show that EA induces both neurogenesis and astrogliogenesis, albeit without qualitative changes compared to the control setting. On the other hand, seizures inhibited neurogenesis by swiftly and drastically altering the fate of newborn cells. In MTLE mice, most of the newborn cells in the SGZ and the GCL were reactive astrocytes (Figures 6A and S5A), i.e., hypertrophic astrocytes that expressed Nestin-GFP in addition to the astrocytic markers GFAP (Figure 6E) or S100-β (data not shown), a marker absent in rNSCs. These newly generated reactive astrocytes are most likely derived from rNSCs as astrocytes were not induced to proliferate in MTLE (Figure 2), and rNSCs acquired a reactive phenotype in parallel to cell division as early as 3 dpKAi (Figures 3 and 4).

The impairment of neurogenesis was obvious in MTLE mice at 50 dpKAi. Because the levels of neuronal hyperactivity and rNSC activation were lower in the EA than in the MTLE mice, rNSC depletion would take longer to manifest. To test this hypothesis, we administered BrdU at 49 dpKAi and sacrificed the mice at 150 dpKAi. The total number of BrdU-positive cells was significantly reduced in EA and especially in MTLE mice (Figures 6B and S5B). As expected, the number of newborn neurons was markedly reduced in MTLE, but also in EA mice. These results confirmed that neuronal hyperexcitation accelerated the depletion of the rNSCs (Figure 5), which translates into decreased neurogenesis, even in the absence of hippocampal pathology. Importantly, the percentage of

newborn neurons and astrocytes was similar in the EA and Sal mice, whereas in MTLE mice, reactive astrocytes accounted for most of the newborn cells in the SGZ and the GCL (Figures 6B, 6E, and S5B).

We next hypothesized that, in MTLE mice, cell proliferation in the DG could not be rescued because the depletion of the rNSC population disrupted the whole neurogenic cascade. To test this hypothesis, we implanted at 50 dpKAi an osmotic minipump to systemically deliver insulin-like growth factor 1 (IGF-1), a strong neurogenic factor (Anderson et al., 2002), for 7 days. BrdU was administered (four injections, 2 hr apart) on the 6th day of IGF-1 treatment, and the mice were sacrificed 24 hr later to assess proliferation (Figure S6A). As expected, IGF-1 increased cell proliferation in Sal mice and was able to restore cell proliferation to control levels in EA mice, but had no significant effect on MTLE mice (Figure S6B). IGF-1 significantly increased the proliferation of ANPs without affecting rNSCs (Figures S6C and 26D***). This explains its effect on EA mice, in which rNSCs and ANPS were still present, albeit at lower numbers than in Sal mice.

Taken together, these results demonstrate that MTLE-induced depletion of the rNSC pool causes a chronic impairment of neurogenesis in the DG. While EA hastens the rNSC depletion that occurs naturally with age, MTLE seizures massively activate and seemingly redirect the rNSCs toward the generation of reactive astrocytes. This cell-fate switch would almost completely deplete the rNSC population and cause the subsequent chronic impairment of neurogenesis in MTLE.

rNSCs Differentiate into Reactive Astrocytes after Seizures

Our differentiation experiments suggested that rNSCs divide and differentiate into reactive astrocytes after seizures. To validate this finding, we subjected tamoxifen-treated Nestin-Cre-ERT2/R26R:YFP transgenic mice to either the EA or to the MTLE protocol (Figure 4) and determined the fate of rNSCs-derived cells at 3, 14, and 30 dpKAi (Figures 7 and S7). We first observed an overtime overall increase in the total number of YFP-expressing cells in the three experimental groups (Figure 7A), an effect that was more pronounced in EA and MTLE mice than in Sal mice, consistent with increased cell proliferation in these two groups (Figure 1). This increase in the total number of YFP-expressing cells was observable as early as at 3 dpKAi, although only reached statistical significance in MTLE mice compared with the Sal group (Figure 7A). With respect to the cell fate of the rNSC-derived cells, no changes were observed at 3 dpKAi. At later time points (14 and 30 dpKAi), we found that most of the rNSC-derived cells were neurons in the Sal and EA groups (Figures 7 and S7A). In contrast, in MTLE mice, the neuronal population was the smallest among the total YFP-expressing population (Figures 7 and S7A). The vast majority of the YFP-expressing cells were reactive astrocytes unambiguously distinguished by their hypertrophic morphology (Figure 7A) and expression of GFAP and S100β (Figures S7B and S7C). Occasional YFP-expressing neurons could be observed in MTLE mice, mainly in the hilar region, confirming the induction of aberrant neurogenesis that we observed in the Nestin-GFP mice (Figure 7A). Our experimental paradigm assures that possible upregulation of nestin in parenchymal astrocytes does not interfere with our results. We activated the inducible expression of GFP by tamoxifen several days prior to the KA injection. Thus, nestin upregulation in astrocytes

due to KA injection could not translate into expression of YFP as nestin expression would start days after tamoxifen administration stopped. The absence of YFP-labeled astrocytes in the molecular layer or the hilus proves this point.

Overall, these results establish that different levels of neuronal hyperexcitation trigger different response from rNSCs. Seizures induced rNSCs to become reactive and to divide symmetrically, generating reactive astrocytes in the DG at the expense of neurogenesis. In contrast, EA induced a marked increase in neurogenesis. However, this pro-neurogenic effect was not sustained over time (Figure 6) because the higher rate of rNSC activation hastened rNSC depletion in the long term (Figure 5). This effect can thus be comparable to accelerated aging of the DG with respect to neurogenesis.

DISCUSSION

In this paper, we provide evidence that different levels of neuronal hyperactivity profoundly affect rNSCs and their progeny, impairing neurogenesis. In a mouse model of MTLE, neuronal hyperexcitation eliciting seizures causes hippocampal rNSCs to become reactive, i.e., to develop a hypertrophic and multibranched phenotype, and getting activated to enter the cell cycle in large numbers. Strikingly, these reactive rNSCs switch to symmetric cell division to generate reactive astrocytes as daughter cells, while in parallel, they directly transform into reactive astrocytes as well. As a result, the neurogenic lineage becomes almost completely abolished. However, neuronal hyperactivity in the form of EA induces more rNSCs to become activated without developing a reactive phenotype or switching to symmetric division, and neurogenesis and astrogliogenesis are transiently enhanced. Nevertheless, EA accelerates the decline of the rNSC population, leading to decreased neurogenesis in the long term. Our results could offer an explanation for the absence of radial nestin-positive cells (putative rNSCs; Blümcke et al., 2001) and the reduction or absence of PSA-NCAM-positive cells (Mathern et al., 2002; Mikkonen et al., 1998; Pirttilä et al., 2005) found in hippocampi from MTLE patients.

The novel properties of rNSCs in response to seizures that we report herein represent a substantial functional shift with critical implications as neurogenesis becomes chronically impaired caused by (1) the fast disruption of the neurogenic cascade as rNSCs stop producing neuronal precursors (ANPs and NBs) and (2) the almost complete depletion of the rNSC pool as they convert into reactive astrocytes. The molecular mechanisms leading to this fate switch remain to be determined, although we speculate that based on the similarities between rNSCs and astrocytes (Seri et al., 2001), the signaling pathway(s) might be similar to those underlying the transformation of astrocytes into reactive astrocytes (reviewed in Sofroniew, 2009). However, our results with the proinflammatory toxin LPS, which does not induce rNSCs to become reactive, suggest the contrary. Finally, our microarray analysis provides a starting point for investigating the specific molecular mechanisms mediating the rNSC responses to different levels of neuronal hyperexcitation.

Our results show that EA alone is sufficient to accelerate the decline of the rNSC population and to diminish neurogenesis in the long term. These results are in agreement with the predictions derived from our model of activation-coupled astrocytic-differentiation of rNSCs

(Encinas et al., 2011b). EA triggers a transient rise in neurogenesis by activating more rNSCs and thus increasing the number of proliferating ANPs, which in turn show enhanced mitotic activity, resulting in increased neurogenesis. As no reactive astrocytes were found and the relative proportion of newborn neurons and astrocytes was similar to basal levels, we argue that EA only exerts a quantitative effect on the neurogenic cascade. Because EA accelerates the depletion of rNSC pool, cell proliferation, neurogenesis, and astrogliogenesis are all eventually reduced below basal levels in the long term. In normal conditions, rNSCs are mostly quiescent, but once activated, they give rise to several neuronal precursors and then differentiate into astrocytes, resulting in a progressive depletion of the rNSC pool (Encinas et al., 2011b). Interestingly, knockout of Ascl1, a transcription factor required to exit quiescence, blocks rNSC activation and preserves the rNSCs population over time (Andersen et al., 2014). Utilizing in vivo clonal analysis based on inducible lineage tracing, rNSCs were found to generate both neurons and astrocytes (Bonaguidi et al., 2011). Remarkably, the authors also found that rNSCs could generate copies of themselves. However, this mechanism for the repopulation of rNSCs does not seem to counteract the depletion of the rNSCs, occurring naturally over time or induced by EA.

We report a long-lasting impairment of neurogenesis in both the EA and the MTLE models. The cognitive functions associated with neurogenesis and the restorative potential to replace the neurons that died due to excitotoxicity will be presumably lost or at least substantially impaired. Based on experimental work using rodents, hippocampal neurogenesis is involved in spatial and associative learning (Clelland et al., 2009; Deng et al., 2009; Dupret et al., 2008; Farioli-Vecchioli et al., 2008; Imayoshi et al., 2008; Saxe et al., 2006), as well as the responses to stress and depression (Snyder et al., 2011), especially in relation to the outcome of antidepressant treatments (Santarelli et al., 2003). It bears mention that epileptic patients have a high incidence of memory impairment (Gargaro et al., 2013) and psychiatric comorbidities, such as anxiety and depression (Heuser et al., 2009). Therefore, it has been speculated that increasing neurogenesis could benefit these patients. Our data, however, suggest a more complicated scenario. Rather than simply increasing neurogenesis, useful therapeutic strategies, assuming similarities between our mode model and humans, should aim at preventing the massive activation of rNSCs and their conversion into reactive astrocytes to prevent the loss of hippocampal neurogenesis.

According to our results, rNSCs may contribute partially to the process of gliosis in the DG. Gliosis, or the formation of a glial scar, is mainly produced by parenchymal astrocytes turning into reactive astrocytes in many neuropathological conditions (Norton et al., 1992; Sofroniew, 2009; Zamanian et al., 2012). Reactive astrocytes have impaired glutamate buffering because of altered expression of glutamate transporters such as GLAST and GLT1, and they produce proinflammatory cytokines with proepileptogenic potential such as IL-1β (Devinsky et al., 2013). Thus, it has been hypothesized that impaired astrocytic function is also a main event in the development of secondary recurrent seizures (Devinsky et al., 2013). Whether the rNSC-derived reactive astrocytes are functionally similar to parenchymal astrocyte-derived reactive astrocytes and contribute functionally to hippocampal sclerosis is an intriguing possibility to be explored in the future.

We conclude that neuronal hyperexcitation leads to long-term impairment of neurogenesis and that the hippocampal neurogenic niche in epilepsy becomes severely disrupted due to a functional switch of rNSCs after seizures. Thus, it could be argued that the regenerative potential and cognitive functions associated with neurogenesis might become compromised. This new insight helps us to better understand the biology of rNSCs and sheds light onto the potential pathophysiological mechanisms underlying MTLE, bringing forward new possibilities for more efficient therapeutic strategies against this devastating neurological disorder.

EXPERIMENTAL PROCEDURES

All animal procedures followed the European directive 2010/63/UE and NIH guidelines following approval from the respective institutional Ethics Committees. All the mice were 2 months old at the time of the intrahippocampal injection of KA and electrode implantation for EEG recording. BrdU administration was always given intraperitoneally, at a concentration of 150 mg/kg of body weight. Four injections, 2 hr apart, were given to each mouse. IGF-1 was administered via an osmotic minipump delivering 50 μg/kg per day of human recombinant IGF-1 per day, for a week. RNA isolation for RT-qPCR included DNase treatment. After the RNA was retrotranscribed, qPCR was performed following MIQE (Minimal Information for Publication of Quantitative Real Time Experiments) guidelines. Multiple-labeling immunohistochemistry, confocal microscopy imaging, and design-based, bias-free stereological quantifications were performed following standard protocols used previously by the authors and optimized for the use with transgenic mice. For statistical analysis, a one-way ANOVA test of all groups was performed to determine the overall effect of each factor if a previous two-way ANOVA (time × factor) had detected interaction between factors. In all cases, all pair-wise multiple comparisons (Holm-Sidak method or Dunn's) were used as a post hoc test to determine the significance between groups in each factor. For analysis of pairs of groups, a Student's t test was performed. Gene expression arrays were performed following MIAME (Minimum Information About a Microarray Experiment) recommendations and were based on protocols and materials provided by Agilent Technologies. Image data from the two-color microarray analysis were extracted and corrected for dye bias and background and further processed for statistical analysis using LIMMA (Linear Model for Microarray Analysis package), and functional analysis (pathway and gene ontology enrichment) was performed. Detailed methods and associated references are provided in as Supplemental Information.

Supplementary Material

Refer to Web version on PubMed Central for supplementary material.

ACKNOWLEDGMENTS

REFERENCES

Altman J, Das GD. Autoradiographic and histological evidence of postnatal hippocampal neurogenesis in rats. J. Comp. Neurol. 1965; 124:319–335. [PubMed: 5861717]

Andersen J, Urbán N, Achimastou A, Ito A, Simic M, Ullom K, Martynoga B, Lebel M, Göritz C, Frisén J. A transcriptional mechanism integrating inputs from extracellular signals to activate hippocampal stem cells. Neuron. 2014; 83:1085–1097. [PubMed: 25189209]

Anderson MF, Aberg MA, Nilsson M, Eriksson PS. Insulin-like growth factor-I and neurogenesis in the adult mammalian brain. Brain Res. Dev. Brain Res. 2002; 134:115–122.

Babb TL, Pereira-Leite J, Mathern GW, Pretorius JK. Kainic acid induced hippocampal seizures in rats: comparisons of acute and chronic seizures using intrahippocampal versus systemic injections. Ital. J. Neurol. Sci. 1995; 16:39–44.

Blümcke I, Schewe JC, Normann S, Brüstle O, Schramm J, Elger CE, Wiestler OD. Increase of nestin-immunoreactive neural precursor cells in the dentate gyrus of pediatric patients with early-onset temporal lobe epilepsy. Hippocampus. 2001; 11:311–321. [PubMed: 11769312]

Bonaguidi MA, Wheeler MA, Shapiro JS, Stadel RP, Sun GJ, Ming GL, Song H. In vivo clonal analysis reveals self-renewing and multipotent adult neural stem cell characteristics. Cell. 2011; 145:1142–1155. [PubMed: 21664664]

Bouilleret V, Ridoux V, Depaulis A, Marescaux C, Nehlig A, Le Gal La Salle G. Recurrent seizures and hippocampal sclerosis following intra-hippocampal kainate injection in adult mice: electroencephalography, histopathology and synaptic reorganization similar to mesial temporal lobe epilepsy. Neuroscience. 1999; 89:717–729. [PubMed: 10199607]

Clelland CD, Choi M, Romberg C, Clemenson GD Jr, Fragniere A, Tyers P, Jessberger S, Saksida LM, Barker RA, Gage FH, Bussey TJ. A functional role for adult hippocampal neurogenesis in spatial pattern separation. Science. 2009; 325:210–213. [PubMed: 19590004]

Deng W, Saxe MD, Gallina IS, Gage FH. Adult-born hippocampal dentate granule cells undergoing maturation modulate learning and memory in the brain. J. Neurosci. 2009; 29:13532–13542. [PubMed: 19864566]

Devinsky O, Vezzani A, Najjar S, De Lanerolle NC, Rogawski MA. Glia and epilepsy: excitability and inflammation. Trends Neurosci. 2013; 36:174–184. [PubMed: 23298414]

Dupret D, Revest JM, Koehl M, Ichas F, De Giorgi F, Costet P, Abrous DN, Piazza PV. Spatial relational memory requires hippocampal adult neurogenesis. PLoS One. 2008; 3:e1959. [PubMed: 18509506]

Encinas JM, Vaahtokari A, Enikolopov G. Fluoxetine targets early progenitor cells in the adult brain. Proc. Natl. Acad. Sci. USA. 2006; 103:8233–8238. [PubMed: 16702546]

Encinas JM, Hamani C, Lozano AM, Enikolopov G. Neurogenic hippocampal targets of deep brain stimulation. J. Comp. Neurol. 2011a; 519:6–20. [PubMed: 21120924]

Encinas JM, Michurina TV, Peunova N, Park JH, Tordo J, Peterson DA, Fishell G, Koulakov A, Enikolopov G. Division-coupled astrocytic differentiation and age-related depletion of neural stem cells in the adult hippocampus. Cell Stem Cell. 2011b; 8:566–579. [PubMed: 21549330]

Eriksson PS, Perfilieva E, Björk-Eriksson T, Alborn AM, Nordborg C, Peterson DA, Gage FH. Neurogenesis in the adult human hippocampus. Nat. Med. 1998; 4:1313–1317. [PubMed: 9809557]

Farioli-Vecchioli S, Saraulli D, Costanzi M, Pacioni S, Cinà I, Aceti M, Micheli L, Bacci A, Cestari V, Tirone F. The timing of differentiation of adult hippocampal neurons is crucial for spatial memory. PLoS Biol. 2008; 6:e246. [PubMed: 18842068]

Fukuda S, Kato F, Tozuka Y, Yamaguchi M, Miyamoto Y, Hisatsune T. Two distinct subpopulations of nestin-positive cells in adult mouse dentate gyrus. J. Neurosci. 2003; 23:9357–9366. [PubMed: 14561863]

Gargaro AC, Sakamoto AC, Bianchin MM, Geraldi Cde.V, Scorsi- Rosset S, Coimbra ER, Carlotti CG Jr, Assirati JA, Velasco TR. Atypical neuropsychological profiles and cognitive outcome in mesial temporal lobe epilepsy. Epilepsy Behav. 2013; 27:461–469. [PubMed: 23611738]

Gibbons MB, Smeal RM, Takahashi DK, Vargas JR, Wilcox KS. Contributions of astrocytes to epileptogenesis following status epilepticus: opportunities for preventive therapy? Neurochem. Int. 2013; 63:660–669. [PubMed: 23266599]

Hattiangady B, Rao MS, Shetty AK. Chronic temporal lobe epilepsy is associated with severely declined dentate neurogenesis in the adult hippocampus. Neurobiol. Dis. 2004; 17:473–490. [PubMed: 15571983]

Hayes NL, Nowakowski RS. Dynamics of cell proliferation in the adult dentate gyrus of two inbred strains of mice. Brain Res. Dev. Brain Res. 2002; 134:77–85.

Heinrich C, Nitta N, Flubacher A, Müller M, Fahrner A, Kirsch M, Freiman T, Suzuki F, Depaulis A, Frotscher M, Haas CA. Reelin deficiency and displacement of mature neurons, but not neurogenesis, underlie the formation of granule cell dispersion in the epileptic hippocampus. J. Neurosci. 2006; 26:4701–4713. [PubMed: 16641251]

Heuser K, Taubøll E, Nagelhus EA, Cvancarova M, Petter Ottersen O, Gjerstad L. Phenotypic characteristics of temporal lobe epilepsy: the impact of hippocampal sclerosis. Acta Neurol. Scand. 2009; (Suppl)(189):8–13.

Hodge RD, Kowalczyk TD, Wolf SA, Encinas JM, Rippey C, Enikolopov G, Kempermann G, Hevner RF. Intermediate progenitors in adult hippocampal neurogenesis: Tbr2 expression and coordinate regulation of neuronal output. J. Neurosci. 2008; 28:3707–3717. [PubMed: 18385329]

Hüttmann K, Sadgrove M, Wallraff A, Hinterkeuser S, Kirchhoff F, Steinhäuser C, Gray WP. Seizures preferentially stimulate proliferation of radial glia-like astrocytes in the adult dentate gyrus: functional and immunocytochemical analysis. Eur. J. Neurosci. 2003; 18:2769–2778. [PubMed: 14656326]

Imayoshi I, Sakamoto M, Ohtsuka T, Takao K, Miyakawa T, Yamaguchi M, Mori K, Ikeda T, Itohara S, Kageyama R. Roles of continuous neurogenesis in the structural and functional integrity of the adult forebrain. Nat. Neurosci. 2008; 11:1153–1161. [PubMed: 18758458]

Kempermann G, Jessberger S, Steiner B, Kronenberg G. Milestones of neuronal development in the adult hippocampus. Trends Neurosci. 2004; 27:447–452. [PubMed: 15271491]

Kralic JE, Ledergerber DA, Fritschy JM. Disruption of the neurogenic potential of the dentate gyrus in a mouse model of temporal lobe epilepsy with focal seizures. Eur. J. Neurosci. 2005; 22:1916–1927. [PubMed: 16262631]

Kronenberg G, Reuter K, Steiner B, Brandt MD, Jessberger S, Yamaguchi M, Kempermann G. Subpopulations of proliferating cells of the adult hippocampus respond differently to physiologic neurogenic stimuli. J. Comp. Neurol. 2003; 467:455–463. [PubMed: 14624480]

Lagace DC, Whitman MC, Noonan MA, Ables JL, DeCarolis NA, Arguello AA, Donovan MH, Fischer SJ, Farnbauch LA, Beech RD, et al. Dynamic contribution of nestin-expressing stem cells to adult neurogenesis. J. Neurosci. 2007; 27:12623–12629. [PubMed: 18003841]

Lugert S, Basak O, Knuckles P, Haussler U, Fabel K, Götz M, Haas CA, Kempermann G, Taylor V, Giachino C. Quiescent and active hippocampal neural stem cells with distinct morphologies respond selectively to physiological and pathological stimuli and aging. Cell Stem Cell. 2010; 6:445–456. [PubMed: 20452319]

Mathern GW, Leiphart JL, De Vera A, Adelson PD, Seki T, Neder L, Leite JP. Seizures decrease postnatal neurogenesis and granule cell development in the human fascia dentata. Epilepsia. 2002; 43(Suppl 5):68–73. [PubMed: 12121298]

Mignone JL, Kukekov V, Chiang AS, Steindler D, Enikolopov G. Neural stem and progenitor cells in nestin-GFP transgenic mice. J. Comp. Neurol. 2004; 469:311–324. [PubMed: 14730584]

Mikkonen M, Soininen H, Kälviänen R, Tapiola T, Ylinen A, Vapalahti M, Paljärvi L, Pitkänen A. Remodeling of neuronal circuitries in human temporal lobe epilepsy: increased expression of

highly polysialylated neural cell adhesion molecule in the hippocampus and the entorhinal cortex. Ann. Neurol. 1998; 44:923–934. [PubMed: 9851437]

Nitta N, Heinrich C, Hirai H, Suzuki F. Granule cell dispersion develops without neurogenesis and does not fully depend on astroglial cell generation in a mouse model of temporal lobe epilepsy. Epilepsia. 2008; 49:1711–1722. [PubMed: 18397295]

Norton WT, Aquino DA, Hozumi I, Chiu FC, Brosnan CF. Quantitative aspects of reactive gliosis: a review. Neurochem. Res. 1992; 17:877–885. [PubMed: 1407275]

Paradisi M, Fernández M, Del Vecchio G, Lizzo G, Marucci G, Giulioni M, Pozzati E, Antonelli T, Lanzoni G, Bagnara GP, et al. Ex vivo study of dentate gyrus neurogenesis in human pharmacoresistant temporal lobe epilepsy. Neuropathol. Appl. Neurobiol. 2010; 36:535–550. [PubMed: 20609110]

Parent JM, Elliott RC, Pleasure SJ, Barbaro NM, Lowenstein DH. Aberrant seizure-induced neurogenesis in experimental temporal lobe epilepsy. Ann. Neurol. 2006; 59:81–91. [PubMed: 16261566]

Pirttilä TJ, Manninen A, Jutila L, Nissinen J, Kälviäinen R, Vapalahti M, Immonen A, Paljärvi L, Karkola K, Alafuzoff I, et al. Cystatin C expression is associated with granule cell dispersion in epilepsy. Ann. Neurol. 2005; 58:211–223. [PubMed: 16049933]

Racine RJ. Modification of seizure activity by electrical stimulation. II. Motor seizure. Electroencephalogr. Clin. Neurophysiol. 1972; 32:281–294.

Sahay A, Wilson DA, Hen R. Pattern separation: a common function for new neurons in hippocampus and olfactory bulb. Neuron. 2011; 70:582–588. [PubMed: 21609817]

Santarelli L, Saxe M, Gross C, Surget A, Battaglia F, Dulawa S, Weisstaub N, Lee J, Duman R, Arancio O, et al. Requirement of hippocampal neurogenesis for the behavioral effects of antidepressants. Science. 2003; 301:805–809. [PubMed: 12907793]

Saxe MD, Battaglia F, Wang JW, Malleret G, David DJ, Monckton JE, Garcia AD, Sofroniew MV, Kandel ER, Santarelli L, et al. Ablation of hippocampal neurogenesis impairs contextual fear conditioning and synaptic plasticity in the dentate gyrus. Proc. Natl. Acad. Sci. USA. 2006; 103:17501–17506. [PubMed: 17088541]

Segi-Nishida E, Warner-Schmidt JL, Duman RS. Electroconvulsive seizure and VEGF increase the proliferation of neural stem-like cells in rat hippocampus. Proc. Natl. Acad. Sci. USA. 2008; 105:11352–11357. [PubMed: 18682560]

Seri B, García-Verdugo JM, McEwen BS, Alvarez-Buylla A. Astrocytes give rise to new neurons in the adult mammalian hippocampus. J. Neurosci. 2001; 21:7153–7160. [PubMed: 11549726]

Sierra A, Encinas JM, Deudero JJ, Chancey JH, Enikolopov G, Overstreet-Wadiche LS, Tsirka SE, Maletic-Savatic M. Microglia shape adult hippocampal neurogenesis through apoptosis-coupled phagocytosis. Cell Stem Cell. 2010; 7:483–495. [PubMed: 20887954]

Snyder JS, Soumier A, Brewer M, Pickel J, Cameron HA. Adult hippocampal neurogenesis buffers stress responses and depressive behaviour. Nature. 2011; 476:458–461. [PubMed: 21814201]

Sofroniew MV. Molecular dissection of reactive astrogliosis and glial scar formation. Trends Neurosci. 2009; 32:638–647. [PubMed: 19782411]

Sofroniew MV, Vinters HV. Astrocytes: biology and pathology. Acta Neuropathol. 2010; 119:7–35. [PubMed: 20012068]

Song J, Zhong C, Bonaguidi MA, Sun GJ, Hsu D, Gu Y, Meletis K, Huang ZJ, Ge S, Enikolopov G, et al. Neuronal circuitry mechanism regulating adult quiescent neural stem-cell fate decision. Nature. 2012; 489:150–154. [PubMed: 22842902]

Spalding KL, Bergmann O, Alkass K, Bernard S, Salehpour M, Huttner HB, Boström E, Westerlund I, Vial C, Buchholz BA, et al. Dynamics of hippocampal neurogenesis in adult humans. Cell. 2013; 153:1219–1227. [PubMed: 23746839]

van Praag H, Schinder AF, Christie BR, Toni N, Palmer TD, Gage FH. Functional neurogenesis in the adult hippocampus. Nature. 2002; 415:1030–1034. [PubMed: 11875571]

Zamanian JL, Xu L, Foo LC, Nouri N, Zhou L, Giffard RG, Barres BA. Genomic analysis of reactive astrogliosis. J. Neurosci. 2012; 32:6391–6410. [PubMed: 22553043]

Highlights

- Kainic acid injections into hippocampus model neuronal hyperactivity in mice

- At low doses, without seizure activity, rNSCs divide asymmetrically

- At high doses, with seizures, rNSCs divide symmetrically into reactive astrocytes

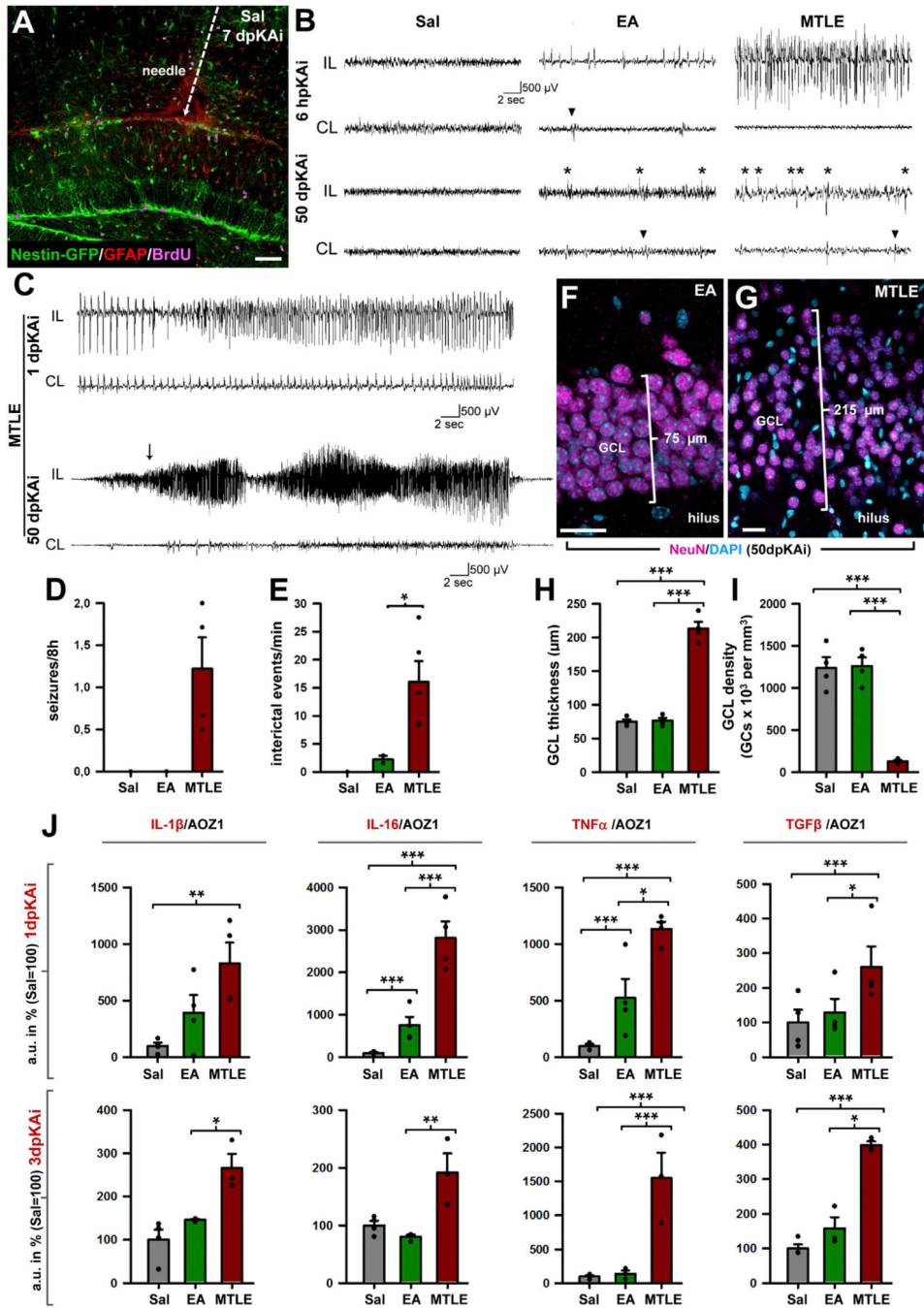- Both models deplete rNSCs and impair hippocampal neurogenesis

Figure 1. Intra-Hippocampal Injection of KA as a Model of EA and MTLE

(A) Confocal image showing the needle track and the place of delivery of Sal/KA into the hippocampus of a Nestin-GFP mouse at 7 dpKAi.

(B) Representative EEG traces from the hippocampus, ipsilateral (IL) and contralateral (CL) to the injection site. During the entire period of monitoring, there were no seizures or interictal spike activity in the saline-treated group (Sal). On the day of the injection, EA mice showed single and brief repetitive trains of spikes activity, and MTLE mice showed seizures. Examples at the 6-hr post-KA injection (6 hpKAi) time point are shown. Abnormal

interictal spike activity (asterisks) was evident in the EA and MTLE mice but not in the Sal group in the days following de KA injection. Examples are provided for the 50-dpKAi time point. Note that less frequent interictal spikes were evident in the CL side (arrowheads).

(C) EEG trace from a MTLE mouse showing electrographic seizures at 1 and 50 dpKAi. The arrow indicates the start of the behavioral seizure recorded on video. Scale bar represents 500 μV/2 s.

(D) Quantification of the average number of seizures per 8 hr (2 to 50 dpKAi). No seizures were detected in the Sal or EA mice.

(E) Quantification of the average number of EA events per minute (2 to 50 dpKAi). In the EA, only epileptiform discharges were detected. In the MTLE, epileptiform discharges occurred with higher frequency. Data are shown from day post-injection (dpi) 0 and 42–50. Bars are shown as mean ± SEM. Dots show individual data. *p < 0.05, after t test (the Sal group was not included as no ictal or interictal activity was recorded).

(F and G) Representative confocal microscopy images showing normal appearance of the GCL in an EA mouse (F) and GCL dispersion and lower neuronal density in a MTLEmouse (G) at 50 dpKAi.

(H and I) Quantification of the GCL thickness, measured as the distance between the hilus and the molecular layer (H), and of the GC (DAPI$^+$ NeuN$^+$ cells) density (I), at 50 dpKAi.

(J) Quantification of the proinflammatory cytokines IL-1β, IL-6, and TNF-α and the anti-inflammatory cytokine TGF-β at 1 dpKAi (upper row) and 3 dpKAi (lower row).

*p < 0.05, **p < 0.01, ***p < 0.001 after all pairwise multiple comparisons by Holm-Sidak post hoc test. Bars show mean ± SEM. Dots show individual data. Scale bar is 50 μm in (A) and 15 μm in (F) and (G).
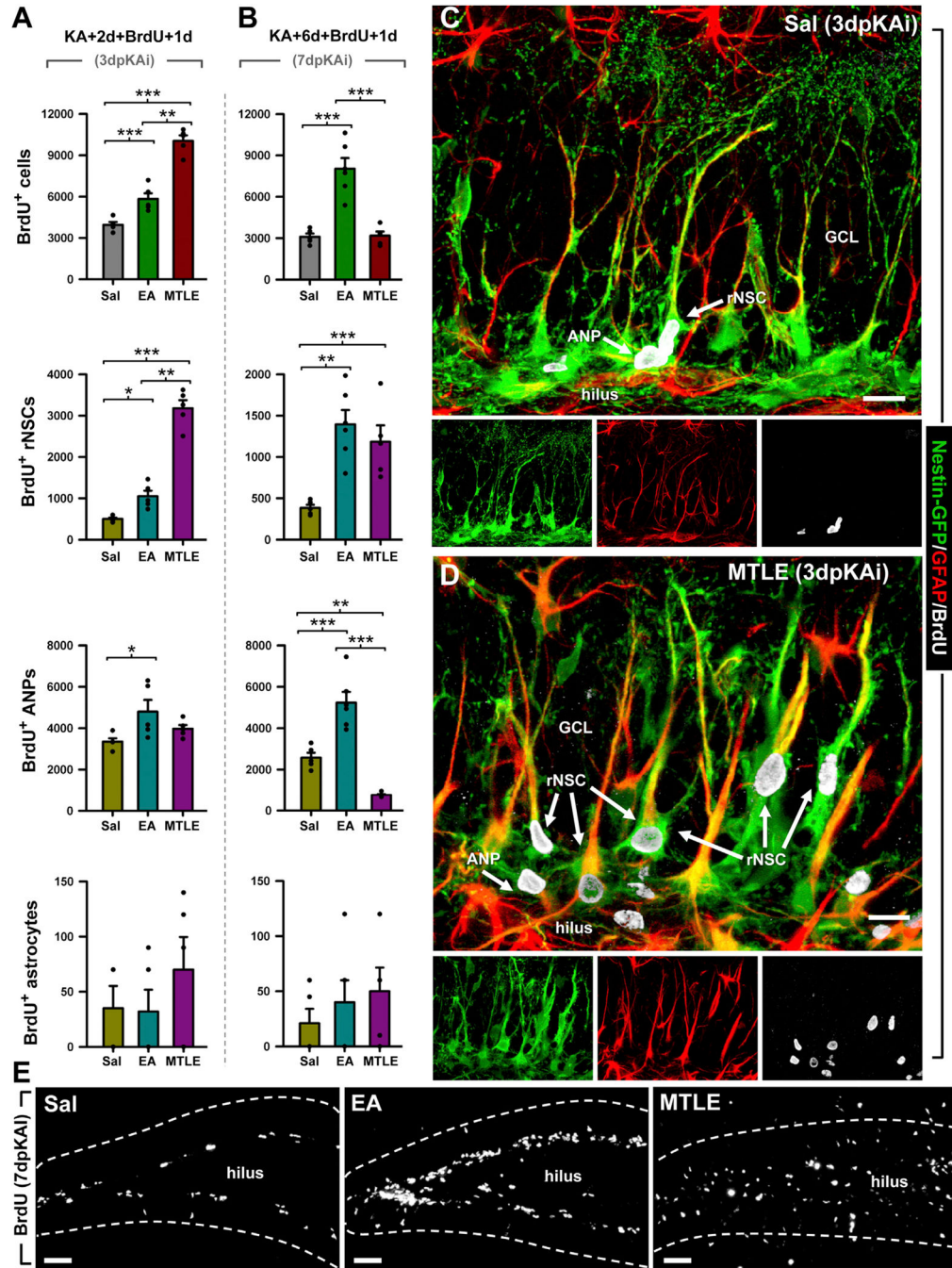
Figure 2. EA and MTLE Promote Cell Proliferation and Activation of rNSCs

(A and B) Quantification at 3 (A) and 7 (B) dpKAi of the absolute number of BrdU+ cells and BrdU-positive rNSCs (Nestin-GFP-positive, GFAP-immunopositive cells with radial morphology located in the SGZ), ANPs (Nestin-GFP-positive, GFAP-negative cells located in the SGZ with short processes with BrdU staining), and astrocytes (Nestin-GFP-negative, GFAP-positive with stellate morphology). $*p < 0.05$, $**p < 0.01$, $***p < 0.001$ by all pairwise multiple comparison by Holm-Sidak post hoc test. Bars show mean ± SEM. Dots show individual data.

(C and D) Representative confocal microscopy images showing the DG from Sal (C) and MTLE (D) Nestin-GFP mice after staining for GFP, BrdU, and GFAP at 3 dpKAi.

(E) Representative images showing cell proliferation in the DG of Sal (left), EA (middle), and MTLE (right) mice at 7 dpKAi. Scale bar is 30 μm in (C) and (D) and 50 μm in (E). GCL, granule cell layer.
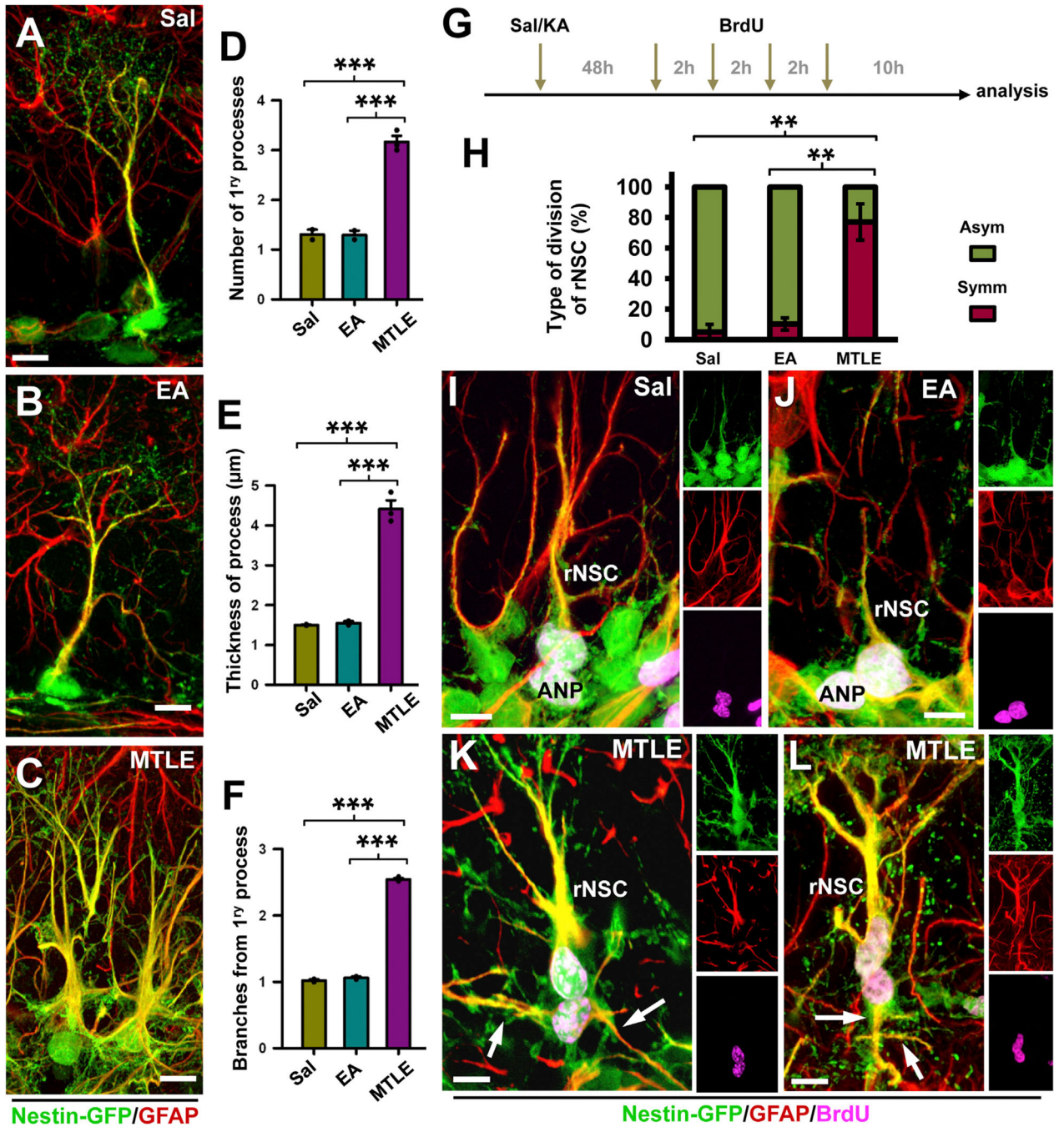
Figure 3. rNSCs Become Reactive as They Divide

(A–C) Confocal microscopy images showing typical rNSCs present in the SGZ of Sal (A) and EA (B) mice and with a reactive phenotype in MTLE (C) mice.

(D–F) Quantification of the number of rNSC primary processes, defined as those emerging from the soma (D), of the thickness, measured as width in projection from z-stacks of rNSC primary processes (E), and of the number of rNSC secondary processes, defined as those branching from the primary process (F).

(G) Experimental paradigm of Sal/KA and BrdU administration designed to increase the probability of capturing cells in telophase, karyokinesis, and cytokinesis.

(H) Quantification of the type of rNSC cell division. "Asymmetric" cell division was assigned when the daughter cell had no processes or short (less than 10 μm) and thin (less than 1 μm) processes lacking GFAP expression. "Symmetric" division was assigned when the daughter cell had clearly defined processes of at least 10 μm in length and 1 μm thickness immunostained for GFAP. Only those pairs of cells with the nucleus still in contact were counted.

(I–L) Confocal microscopy images showing typical asymmetric division of rNSCs in Sal (I) and EA (J) mice and symmetric division in MTLE mice (K and L).

The arrows point at GFAP-immunostained processes of the daughter cells. Scale bar is 10 μm in (A), (B), (H), and (I) and 20 in (C), (J), and (K). **$p < 0.01$, ***$p < 0.001$ by all pairwise multiple comparison by Holm-Sidak post hoc test. Bars show mean ± SEM. Dots show individual data.
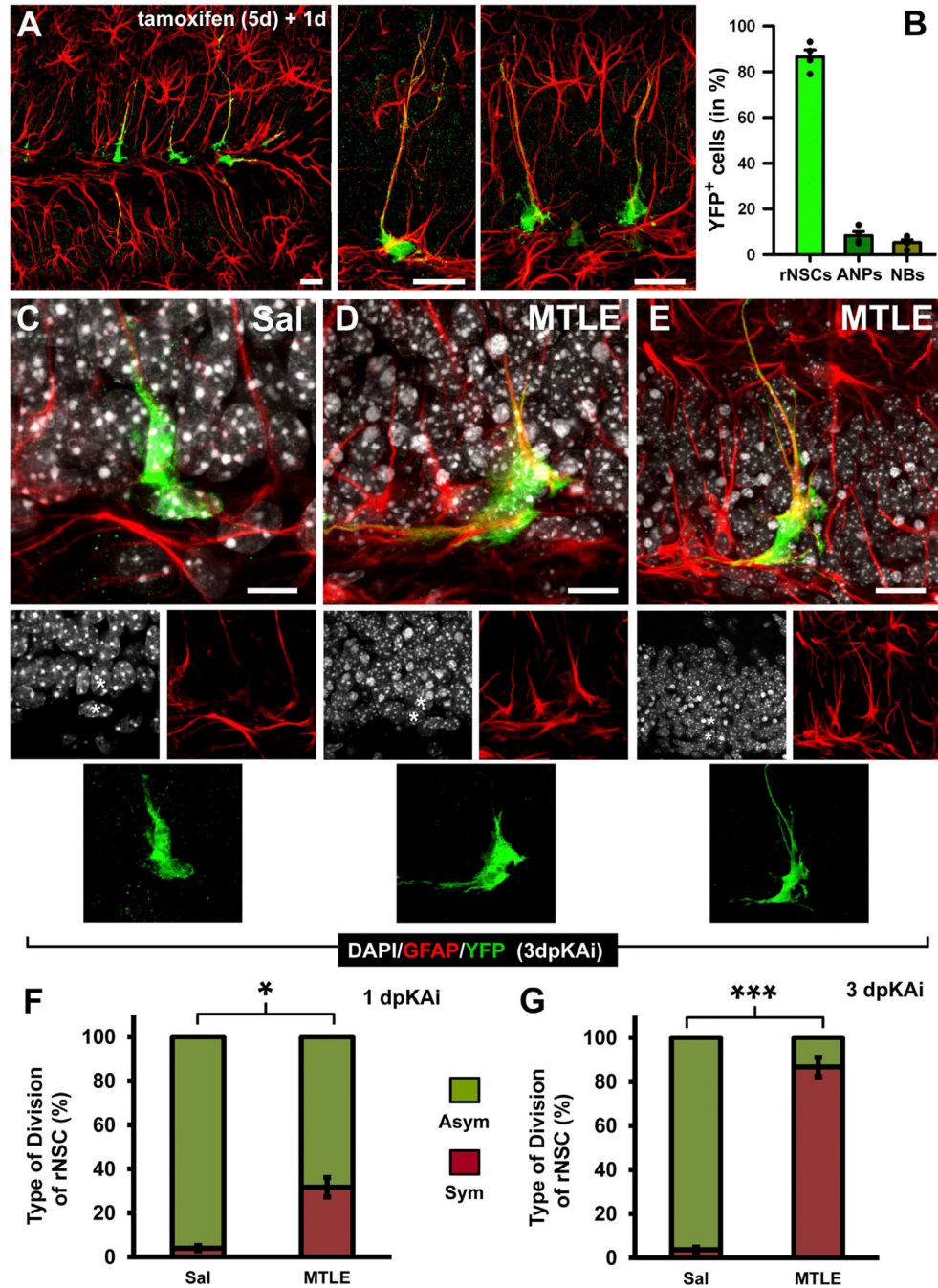
Figure 4. Reactive rNSCs Divide Symmetrically

(A) Confocal microscopy images (projection from z-stacks) showing activation of YFP expression in rNSCs in the DG of inducible nestin-CreERT2/R26R:YFP transgenic mice. The animals received a daily injection of tamoxifen for 5 days and were sacrificed 1 day after the last injection.

(B) Quantification of YFP-expressing cells at 1 day after the last injection of tamoxifen.

(C–E) Confocal microscopy images of pairs of cells undergoing cell division (note that the cytoplasm is still united) in Sal (C) and MTLE mice at 1 (D) and 3 (E) dpKAi. Sal/KA was

injected 3 days after tamoxifen treatment was completed to avoid potential de novo expression of nestin (and YFP) in reactive parenchymal astrocytes, which would interfere with the results. The asterisks indicate the nuclei of the YFP^{+} cells.

(F and G) Quantification of the type of cell division of YFP-expressing rNSCs at 1 (F) and 3 dpKAi (G) time points. The "asymmetric" category was assigned when the daughter cell had no processes, or short (less than 10 μm) and thin (less that 1 μm) processes lacking GFAP expression, as in (C). The "symmetric" category was assigned when the daughter cell expressed GFAP and had at least one long (more than 20 μm) cytoplasmic process.

Scale bars are 20 μm in (A), 10 μm in (C) and (D), and 15 μm in (E). *$p < 0.05$ and ***$p < 0.001$ by Student's t test. Bars show mean ± SEM.
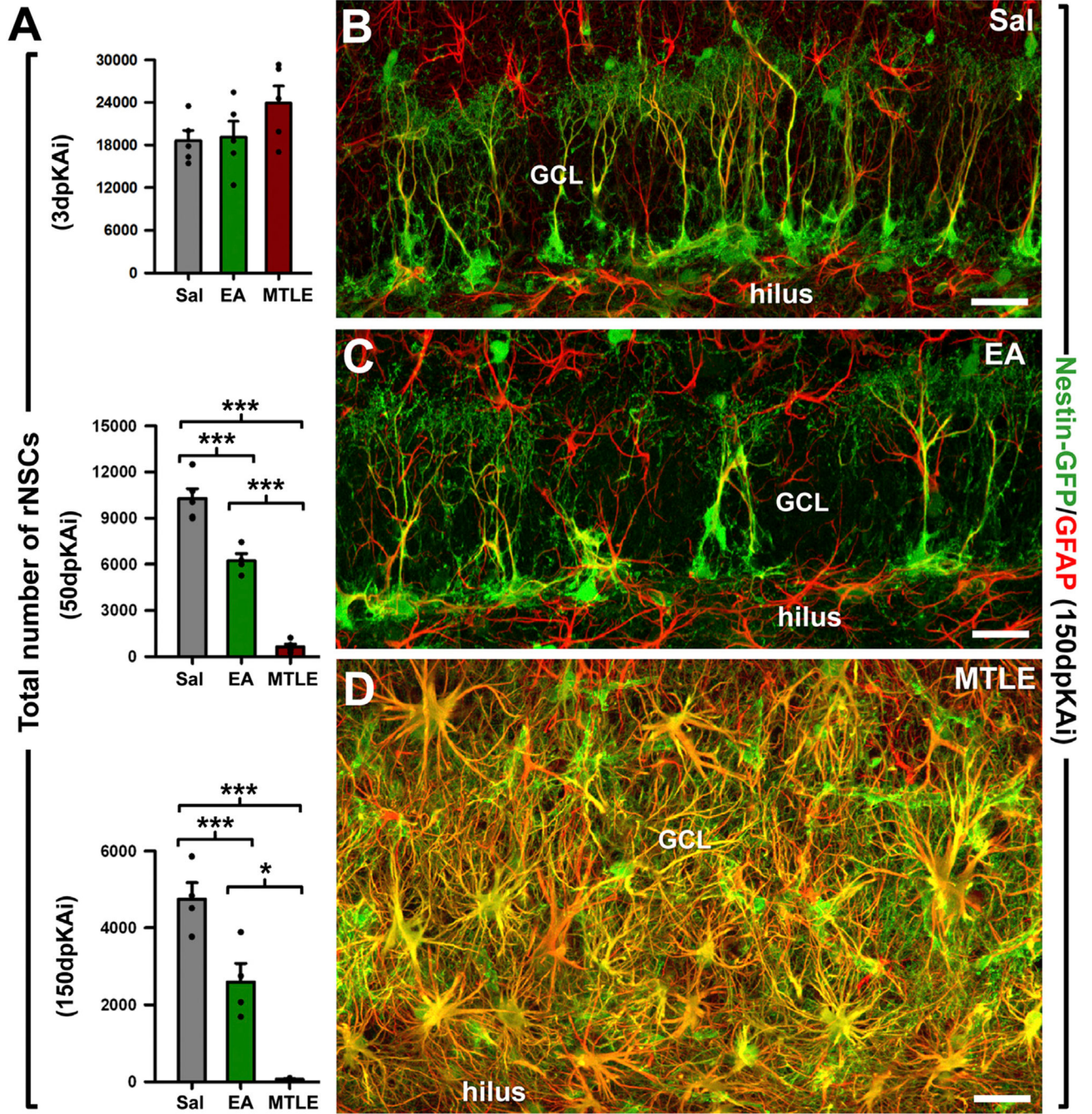
Figure 5. EA and MTLE Deplete the rNSC Population

(A) Quantification of rNSCs (defined as Nestin-GFP cells whose soma was located in the SGZ and with a radial process immunostained for GFAP crossing the GCL) at 3, 50, and 150 dpKAi. Note the difference in the y axis scale across different time points examined. *p < 0.05, ***p < 0.001 by all pairwise multiple comparison by Holm-Sidak post hoc test. Bars show mean ± SEM. Dots show individual data.

(B–D) Representative confocal microscopy images from the DG of Sal (B), EA (C), and MTLE (D) Nestin-GFP mice after staining GFP and GFAP at 150 dpKAi. Scale bar is 40 μm in all images. GCL, granule cell layer.
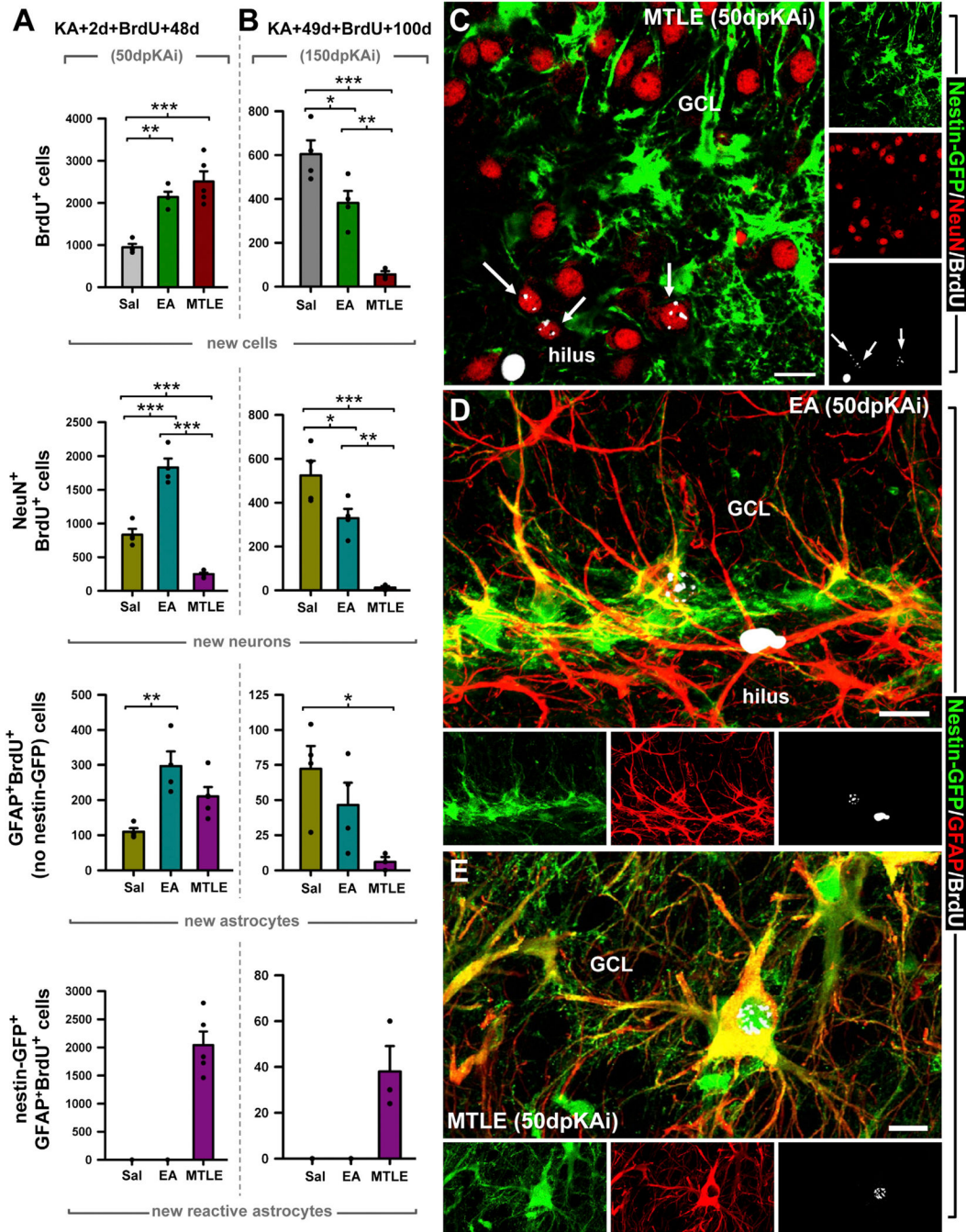
Figure 6. EA and MTLE Impair Neurogenesis in the Long Term

(A and B) Quantification of the absolute number of BrdU+ cell; and newborn neurons (NeuN+BrdU-labeled cells), astrocytes (GFAP+BrdU+-labeled cells negative for Nestin-GFP), and reactive astrocytes (GFAP+Nestin-GFP+BrdU+-labeled cells with hypertrophic cytoplasm) at 50 dpKAi, with BrdU injected 2 days after the KA injection (A), and at 150 dpKAi, with BrdU injected 49 days after the KA injection (B). Note the difference in y axis scale across different cell types analyzed. *p < 0.05, **p < 0.01, ***p < 0.001 by all pair-wise multiple comparison by Holm-Sidak post hoc test. For new reactive astrocytes, a

Dunn's all pair-wise test was performed. Bars show mean ± SEM. Dots show individual data.

(C) Representative example of a MTLE Nestin-GFP DG immunostained for GFP, BrdU, and NeuN at the 50-dpKAi time point. The confocal-microscopy projection of a 15-μm-thick stack shows the abnormal location of newborn neurons.

(D) Example of a newborn astrocyte with its characteristic star-like morphology in the SGZ of an EA mouse.

(E) Example of a newborn reactive astrocyte with its characteristic features: hypertrophic soma, thickened processes, and overexpression of GFAP in the GCL of an MTLE mouse. Scale bar is 30 μm in all images. GCL, granule cell layer.
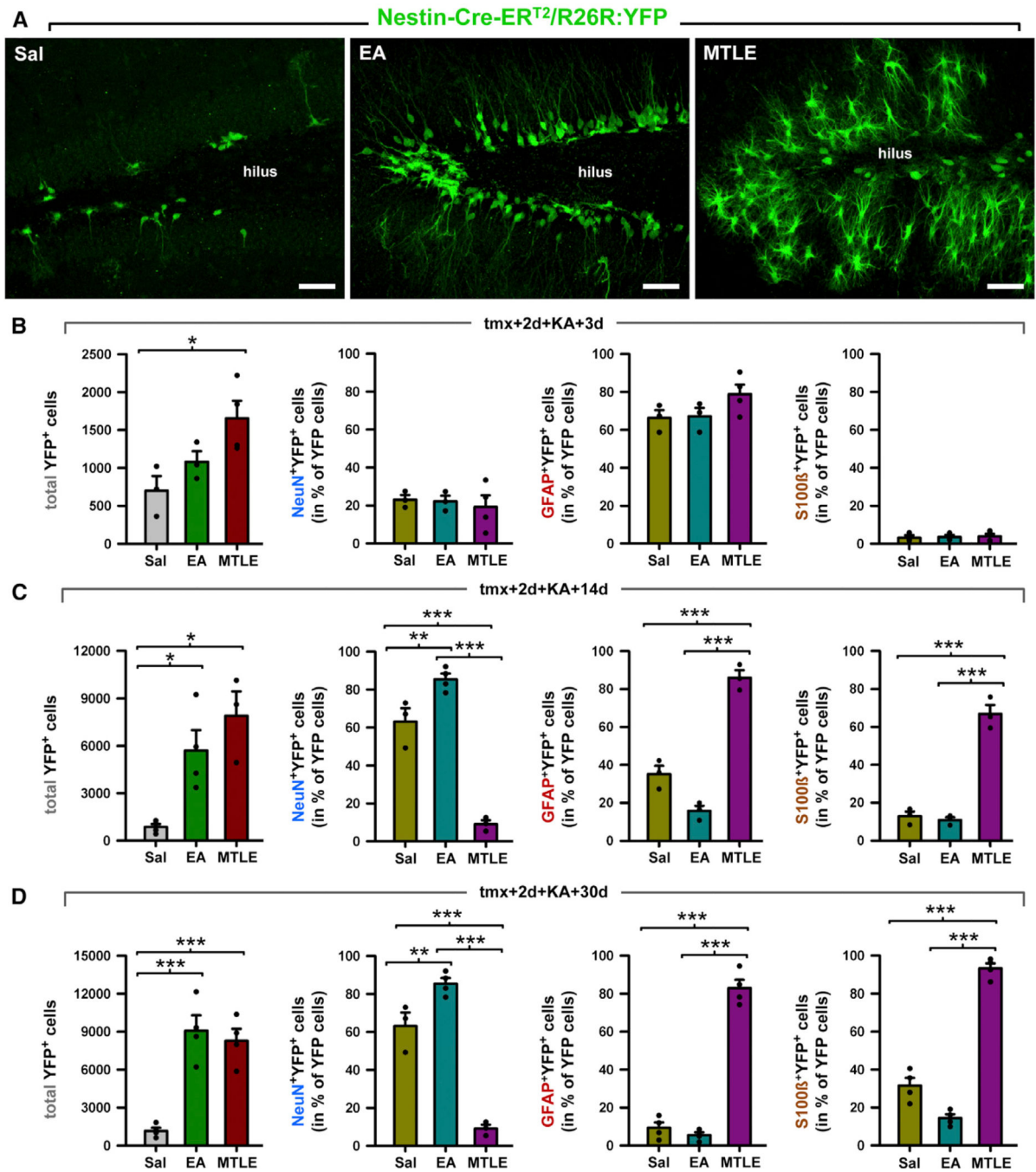
Figure 7. Neurogenesis and Astrogliogenesis in Inducible Nestin-CreER(T2)/R26R:YFP Transgenic Mice

(A) Confocal microscopy images from 20-μm-thick z stacks of the DG after staining for YFP show the neurogenic effect of EA and the reactive-astrogliogenic effect of MTLE at 30 dpKAi.

(B–D) Quantification of the absolute number of YFP+ cells and the relative number of YFP+ cell types at 3 dpKAi (B), 14 dpKAi (C), and 30 dpKAi (D). The total number of YFP-positive cells increased significantly in the EA and MTLE mice in comparison to the Sal group. The neuronal fate of YFP+ cells (number of NeuN+YFP+ cells) was significantly

promoted in EA mice, whereas the astroglial fate (GFAP$^+$YFP$^+$ or S100β$^+$YFP$^+$) was favored in MTLE mice.

$*p < 0.05$, $**p < 0.01$, $***p < 0.001$ by all pairwise multiple comparisons by Holm-Sidak post hoc test. Bars show mean ± SEM. Dots show individual data.